JOURNAL OF THE KOREAN ASTRONOMICAL SOCIETY
38: 33 ~ 41, 2005

A STUDY OF MOLECULAR CLOUD ASSOCIATED WITH THE H II REGION Sh 156

MEEJOO KANG[1,2], AND YOUNGUNG LEE[2]
[1]Department of Astronomy & Space Science, Chungnam National University, Daejeon 305-764, Korea
[2] Korea Astronomy and Space Science Institute, Taeduk Radio Astronomy Observatory, Daejeon 305-348, Korea
E-mail:mjkang@trao.re.kr
(Received January 31, 2005; Accepted April 20, 2005)

ABSTRACT

We have conducted observations toward the molecular cloud associated with the H II region Sh 156 in ^{13}CO($J = 1-0$), C^{18}O($J = 1-0$), and CS($J = 2-1$) using the TRAO 14 m telescope. Combining with existing ^{12}CO($J = 1-0$) data of the Outer Galaxy Survey, we delineated the physical properties of the cloud. We found that there is a significant sign of interaction between the H II region and the molecular gas. We estimated the masses of the molecular cloud, using three different techniques; the most plausible mass is estimated to be $1.37 \times 10^5 M_\odot$, using a conversion factor of $X = 1.9 \times 10^{20}$ cm^{-2} (K km s^{-1})$^{-1}$, and this is similar to virial mass estimate. This implies that the cloud is gravitationally bound and in virial equilibrium even though it is closely associated with the H II region. In addition to existing outflow, we found several MSX and IRAS point sources associated with dense core regions. Thus, more star forming activities other than the existing H II region are also going on in this region.

Key words : H II region - ISM : molecular lines - ISM : individual objects : Sh 156

I. INTRODUCTION

Star formation activities surely have a profound effect on the surrounding interstellar medium. Many efforts have been devoted to observing interaction between the H II regions and their parental molecular clouds by molecular line spectroscopy (Lada et al. 1978; Elmegreen & Moran 1979; Keto & Ho 1989). Some evidence has been presented showing that molecular material near H II regions may be disturbed by several km s^{-1} (Elmegreen & Wang 1987). The evolution of remnant clouds, however, have not been studied in enough detail.

The Sharpless 156 (IC1470), located at $(l, b) = (110.°11, +0.°05)$, is a compact H II region associated with an extensive molecular cloud in the Perseus arm. This object has been relatively well studied at optical and infrared radiation, as it shows a strong emission at both radiation range (Blair et al. 1975; Lynds & O'Neil 1983; Cohen & Barlow 1973; Barlow et al. 1976; Smutko & Larkin 1999). Heydari-Malayeri et al. (1980) notified that the observed ionization structure seems to be in good agreement with the O 7V spectral type of the exciting star in their optical wavelengths study: In their picture, the ionizing star lies outside the molecular cloud. This view is in good agreement with that of another optical study by Lynds & O'Neil (1983), who found a velocity gradient across the cloud of a few km s^{-1}. Based on this and additional data set, Lynds & O'Neil (1983) suggested that Sh 156 sit at the edge of a molecular cloud and could be well described by the champagne model of Tenorio-Tagle (1979). Heydari-Malayeri et al. (1980) found no evidence for a shock front; however, their photographic data showed only the brightest central region of Sh 156, but not the more extended structure. On the other hand, only limited studies at millimeter-wavelength radiation had been reported for the cooler gas: Blitz et al. (1982) found $V_{CO} = -51$ km s^{-1} and $\Delta V_{CO} = 4.6$ km s^{-1}, while Fich et al. (1990) find $V_{H\alpha} = -52.9$ km s^{-1} with $\Delta V_{H\alpha} = 40.1$ km s^{-1} from their one-point Hα observation, respectively. To study the interaction phenomena of the molecular clouds and H II region as well as the global physical properties of the gas, it is necessary to map the extended region in high resolution using molecular gas tracers, such as ^{12}CO and ^{13}CO.

In this paper, we present the results of observations towards Sh 156 and its associated molecular cloud, mapped in ^{12}CO, ^{13}CO, C^{18}O and CS to clarify above mentioned issues. In section II, we describe details of the observational methods, data taking. In Section III, we present the results of observations, including morphology, kinematics, and derive its physical parameters. In Section IV, we discuss the results of gas properties, the star forming activities, and the observational evidence for the interactions between the H II region and the molecular cloud. We summarize our results and analysis in Section V.

II. OBSERVATIONS

Firstly, we obtained ^{12}CO ($J = 1-0$) data from the FCRAO CO Survey of the Outer Galaxy (Heyer et al. 1998). The FCRAO CO Survey of the Outer Galaxy is comprised of 1,696,800 spectra sampled every 50″ covering $l = 102.°49$ to $141.°54$, and $b = -3.°03$ to

Corresponding Author: M. Kang

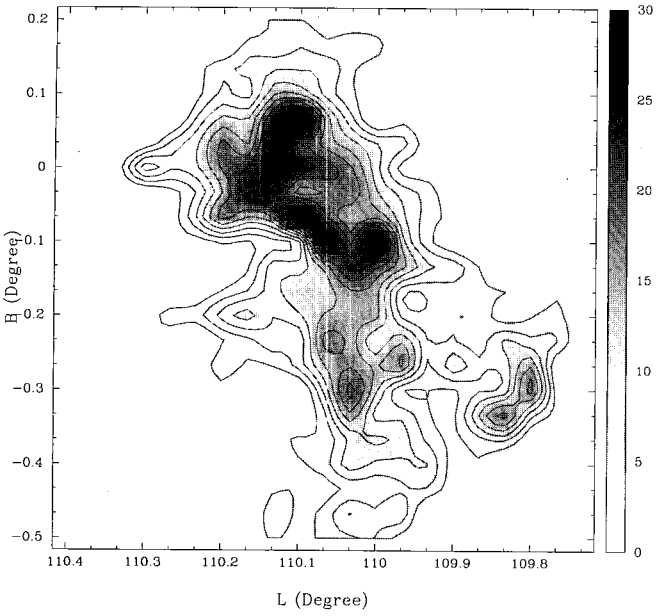

Fig. 1.— The ^{13}CO integrated intensity map of the Sh 156 molecular cloud in the velocity range from −55.10 to −44.90 km s^{-1}. The starting contour is 5 K km s^{-1}, and the contour increment is 2 K km s^{-1}. The grey scale bar is presented in units of K km s^{-1}.

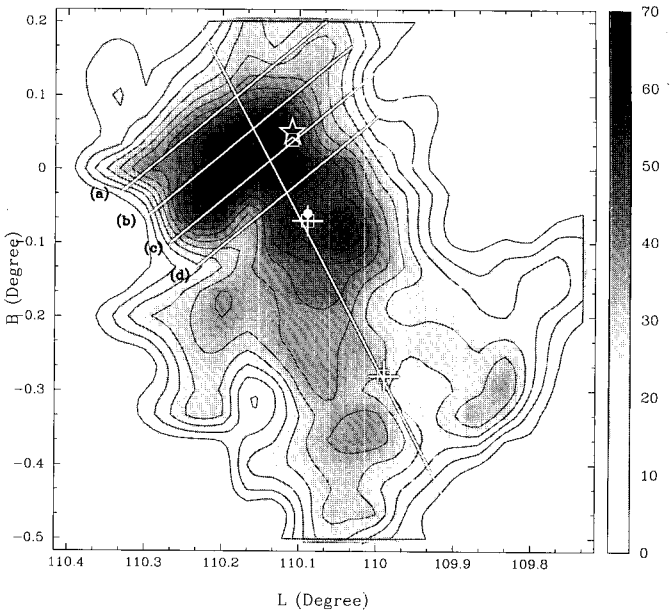

Fig. 2.— The ^{12}CO integrated intensity map in the velocity range from −55.28 to −44.72 km s^{-1}. The starting contour is 10 K km s^{-1}, and the contour increment is 5 K km s^{-1}. Star symbol represents the H II region Sh 156, open squares for H_2O masers (Valdettaro et al. 2001), filled circle for high-mass protostellar candidate (Williams et al. 2004), and plus symbols for molecular outflow sources (Wouterloot et al. 1989). The grey scale bar is presented in units of K km s^{-1}. The oblique line from the southwest to the northeast direction shows the section for the position-velocity map presented in Figure 7. The oblique lines from the southeast to the northwest direction show the sections for the position-velocity maps in Figure 8.

5.°41. The selected region is about 40′ × 42′ centered on Sh 156. From 2003 to 2004 season, we mapped a 40′ × 42′ region including Sh 156, in ^{13}CO($J = 1 - 0$), using the 3 mm receiver on the 13.7 m Taeduk Radio Astronomy Observatory (TRAO) telescope on a 2′ grid. The beam size is 53″. We also made supplementary observation of high density tracers, CS($J = 2 - 1$), C^{18}O($J = 1 - 0$) for the bright ^{13}CO($J = 1 - 0$) emission region. The rest frame line frequencies are 97.980968 GHz for CS($J = 2 - 1$), and 109.782182 GHz for C^{18}O($J = 1 - 0$). Two 256-channel filterbanks, with a spectral resolution of 250 kHz, were used. This provided velocity resolution of 0.68 km s^{-1} at the frequency of ^{13}CO($J = 1 - 0$). All antenna temperatures have been corrected for atmospheric extinction, as well as for the forward spillover and scattering losses of the antenna and radome ($\eta_{fss} = 0.63$ at 85-115 GHz (Roh & Jung 1999)). Therefore all temperatures are on the T_R^* temperature scale defined by Kutner and Ulich (1981). The average rms noise of the data is 0.22 K for ^{13}CO($J = 1 - 0$). The average system temperature was 510 K. The obtained ^{12}CO($J = 1 - 0$) data cube were resampled on 2′ grid, matching the pixel sizes of ^{13}CO($J = 1 - 0$) cube data.

We have acquired IRAS Sky Survey Atlas image at 100 μm IRAS band and Midcourse Space Experiment (MSX) image at 8.28 μm , centered on (l, b) = (110°, +0.°05) from Infrared Processing and Analysis Center (IPAC) using Skyview Virtual Observatory (http://skyview.gsfc.nasa.gov/skyview.html), and examined the dust emission distribution of the region.

Using an AIPS task HGEOM, we transforms IRAS image so that its geometry as described by the header is consistent with that of our ^{13}CO($J = 1 - 0$) map for comparison.

III. RESULTS

(a) Cloud Morphology

The ^{13}CO integrated intensity map of the molecular cloud is presented in Figure 1. Most of the emission appears at $V_{\rm LSR}$ from −55.10 to −44.90 km s^{-1}. Figure 2 shows the integrated intensity map of ^{12}CO at $V_{\rm LSR}$ from −55.28 to −44.72 km s^{-1}. The cloud is elongated along the northeast-southwest direction, extended about 21′ × 42′. Using an adopted distance of 3.5 kpc (Hunter & Massey 1990; see below), the full extent of the cloud is estimated to be 21.4 pc × 42.8 pc. The previously archived data points obtained from Centre de Donnes astronomiques de Strasbourg (CDS) within our observing region are overlayed in Figure 2. In this figure, Molecular outflows and H_2O maser sources are located at the same positions, implying these are regions of relatively high mass star

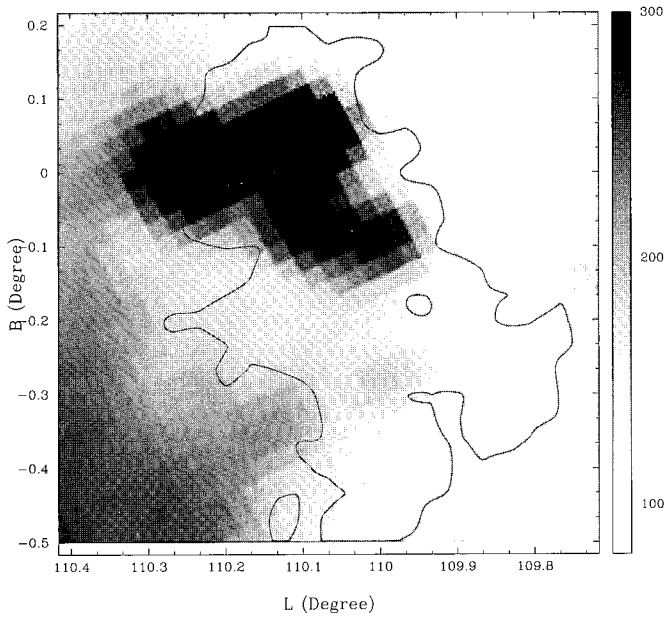

Fig. 3.— The IRAS image at 100 μm. The grey scale bar is presented in units of MJy/steradian. The contour is 5 K km s^{-1} of ^{13}CO integrated intensity, representing silhouette of the molecular cloud.

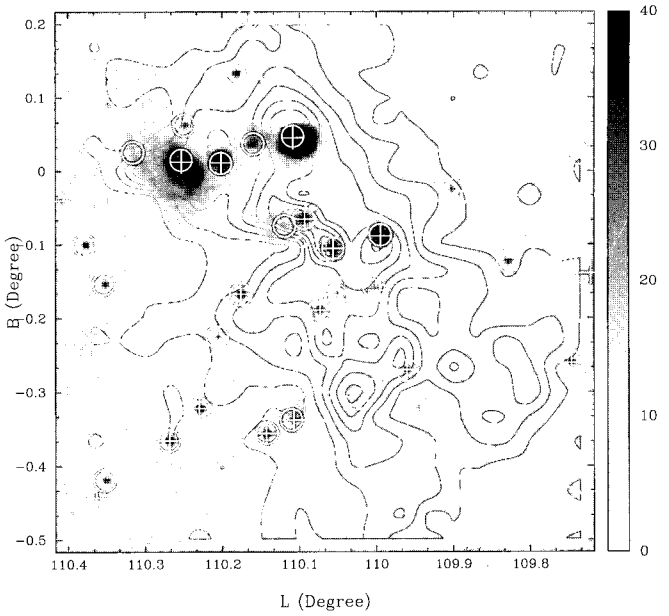

Fig. 4.— The ^{13}CO peak temperature map overlaid on the MSX 8.28 μm image. The starting contour is 0.8 K, and the contour increment is 1 K. Crosses : IRAS point sources, open circles : MSX point sources. The grey scale bar is presented in units of 10^{-7} Wm^{-2}sr^{-1}.

formation.

Determination of distance to the target cloud is critical for estimating several physical parameters. However, there is a substantial difference between the kinematic and spectroscopic distances to Sh 156, ranging from 6.4 kpc to 3.5 kpc. (Lynds & O'Neil 1983). In fact, this is not surprising as the distance estimate for a number of other H II regions in the Perseus Arm usually has large uncertainty. Hunter & Massey (1990) suggested the distance of Sh 156 was 5.3 kpc. This was taken to be the average of the kinematic and stellar distance. The kinematic distance of Sh 156 is determined 4.5 kpc, using our ^{12}CO velocity and the Schmidt (1965) model. But the kinematic distance in this longitude direction has large uncertainty as the rotation curve outside the solar circle is not well-determined. Recently, Barbon & Hassan (1996) estimated its distance as 3.09 kpc using UBV photometry. The most recently cited distance is 3.5 kpc (Wu et al. 2004). Thus, we select a distance of 3.5 kpc to the H II region Sh 156 and its associated molecular cloud.

In Figure 3 we present the IRAS flux map at 100 μm . The ^{13}CO integrated intensity contour at about 3σ (5 K km s^{-1}) is overlayed to show the silhouette of the cloud. As the target region is located in Galactic plane, the correlation between CO and dust emission is not noticeable, except the directly heated area around the H II region. To see more detailed dust emission we examined the MSX image. Figure 4 is an MSX image at 8.28 μm , and the contour map of ^{13}CO peak temperature is overlayed. The ^{13}CO peaks seem to be roughly matching with MSX emission peaks. Many of embedded infrared sources are associated with peak emission in the ^{13}CO, especially around (l, b) = (109.°95 to 110.°15, −0.°1). It is likely that star formation may occur in these sources. It is very noticeable that there is another strong MSX point source at (l, b)=(110.°25, 0.°0), except the H II region Sh 156, the continuum emission of which is also relatively strong at 11cm emission (Fürst et al. 1990).

(b) Velocity Field

The velocity field of the molecular cloud are shown in channel maps of Figures 5, and 6. The ^{13}CO data were resampled 0.8125 km s^{-1} per channel, matching the velocity resolution of the ^{12}CO data, and two channels are binned and presented in each panel. Though the entire observed velocity range extends from $V_{\rm LSR}$ = −136.70 km s^{-1} to 37.38 km s^{-1}, we present here only the velocity range with significant ^{12}CO emission from $V_{\rm LSR}$ = −55.28 km s^{-1} to −44.72 km s^{-1}. It is likely that molecular gas is disturbed only by the residing H II region, $V_{\rm LSR}$ of which is −51.1 km s^{-1}. The strongest molecular emission arises in this region. This velocity is not much different from that of the ionized gas measured by H$_\alpha$ ($V_{\rm LSR}$ = −51.7 km s^{-1} ; Crampton et al. 1978). Fich et al. (1990) find V$_{H\alpha}$ = −52.9 km s^{-1} with Δ V$_{H\alpha}$ = 40.1 km s^{-1}. This suggests that the optical H II region is physically associated with the observed molecular gas. This issue will be discussed in later section.

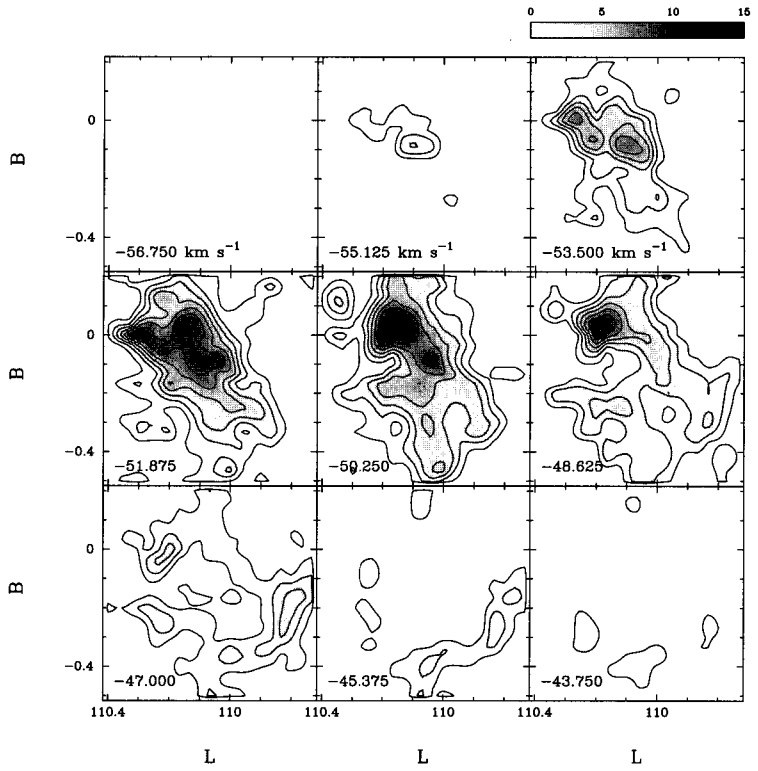

Fig. 5.— The ^{12}CO channel maps with a velocity interval of 1.625 km s^{-1}. The starting contour is 1.5 K km s^{-1}, and the contour increment is 1.5 K km s^{-1}.

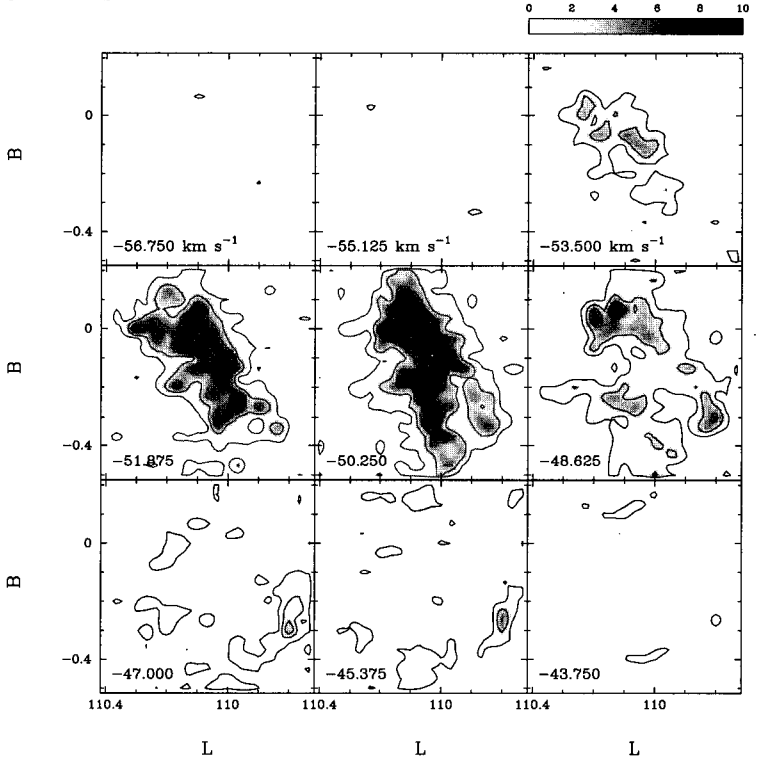

Fig. 6.— The ^{13}CO channel maps with a velocity interval of 1.625 km s^{-1}. The starting contour is 0.5 K km s^{-1}, and the contour increment is 1.0 K km s^{-1}.

In the meanwhile, there is a small cloud, which is elongated from the south to the west in the bottom part, seems to an independent cloud, as its velocity is about -47 km s^{-1}, quite different from the main cloud.

A position-velocity map is presented in Figure 7, which cuts through the whole cloud including the H II region from the southwest to the northeast direction (a long solid line in Figure 2). Figure 8 is the position-velocity maps which cut four sections around the H II region Sh 156 from southeast from northwest direction (a-d in Figure 2). These position-velocity maps show a significant sign of the disturbance; There is a broadened velocity range around the H II region, implying that the molecular cloud is directly affected by the stellar wind from the H II region Sh 156. In fact, other evidence of the association of the molecular cloud was provided by the radial velocity measurement of the ionized gases, $V_{H\alpha} = -52.9$ km s^{-1} (Fich et al. 1990), as mentioned in section I.

(c) Mass

We have estimated cloud mass in three different methods: a mass estimate using virial assumption, an LTE mass assuming LTE condition, and $M_{\rm CO}$, a mass estimate obtained by using the empirical relationship between the CO integrated intensity and molecular hydrogen column density, or equivalently, the relationship between CO luminosity and mass. More detailed discussion of these technique and assumption inherent in its use can be found in several other papers (Lee 1994; Dickman 1978).

In the LTE technique, the assumptions are as follows : ^{12}CO is optically thick, the molecules along the line of sight possess a uniform excitation temperature, the excitation temperature of the two isotopic species are equal and the cosmic background radiation is no important. With these assumptions, the common excitation temperature T_{ex} can be obtained from the peak ^{12}CO antenna temperature. The column density of ^{13}CO at each map position is determined by the ^{12}CO and ^{13}CO line temperatures and the linewidth of the ^{13}CO emission. The detailed process of estimating that column density can be found in Lee (1994). The derived molecular mass (including helium) is $1.19 \times 10^5 M_\odot$.

We also derived the viral mass of the ^{12}CO. If a molecular cloud is gravitationally bound, and has had enough time to be dynamically relaxed, then the partition of energy will be governed by the virial theorem. The total kinetic energy of the molecular cloud is equal to minus 1/2 times the total gravitational potential energy. In other words, the potential energy must equal the kinetic energy, within a factor of two. From this relation, the virial mass is given by

$$M_{VIR} = \frac{3\beta\sigma_{tot}^2}{2G} D, \qquad (1)$$

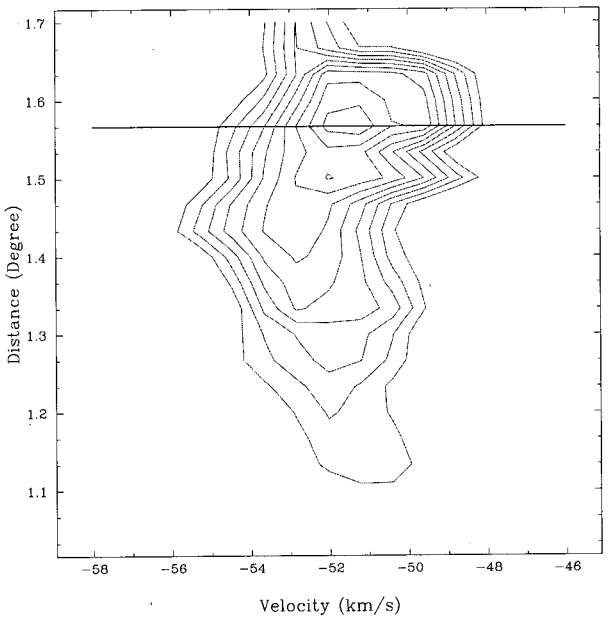

Fig. 7.— The ^{12}CO position-velocity map through a section of the H II region. The straight line represents the H II region Sh 156 . The starting contour is 4 K and the contour increment is 1 K. The solid line represents the position of H II region Sh 156.

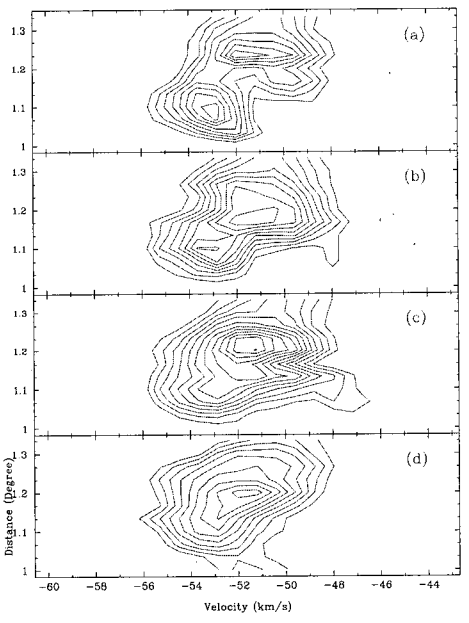

Fig. 8.— The ^{12}CO position-velocity maps of four sections of the H II region presented in Figure 2. The starting contour is 2.5 K and the contour increment is 1 K.

Where D is cloud diameter, and σ_{tot} is total velocity dispersion of the cloud, which represents all forms of kinetic motion within the cloud. Thus, the total velocity dispersion of a cloud can be represented by $\sigma_{tot} = \sqrt{\sigma_i^2 + \sigma_c^2}$. The centroid velocity dispersion (σ_c) is simply the ensemble variance of the line of sight average velocities (Lee 1994). The internal velocity dispersion (σ_i) characterizes the magnitudes of gas motions along individual lines of sigh with respect to the average velocities along those directions. The constant β is usually dependent on the density model of the cloud. Here, we assumed a uniform density distribution and a spherical cloud. The derived virial mass is $1.41 \times 10^5 M_\odot$.

A third technique for estimating cloud masses is by using the relationship between the CO integrated intensity and the molecular hydrogen column density, for equivalently that between CO luminosity (L_{CO}) and gas mass (M_{CO}). The proportionality constant X is then a conversion factor from CO luminosity (or integrated intensity) to gas mass (or column density); it is implicitly assumed that such a factor has general applicability. We have used an estimate of this conversion factor: $X = 1.9 \times 10^{20}$ cm^{-2} (K km s^{-1})$^{-1}$ (Strong & Mattox 1996). The derived mass is $1.37 \times 10^5 M_\odot$.

(d) The Outflows

We have detected the broadened ^{12}CO emission wings toward IRAS 23032+5937 and confirmed the outflow feature which was also studied by Hodapp (1994). He conducted a K′−band imaging survey with a $\approx 8' \times 3'$ field of view of all regions with CO molecular outflow. We show the composite spectra of ^{12}CO and ^{13}CO together in Figure 9. The spectra are generated with the velocity resolution of 0.8125 km s^{-1}. The position of the IRAS point source is marked as asterisk. The outflow seems to be affecting the surrounding molecular cloud; Line profiles around the outflow (spectra marked as asterisk) are broader than those of other parts. The molecular outflow phenomenon represents an evolutionary stage earlier than pre-main-sequence stars manifested as visible T Tauri stars or Herbig Ae/Be stars. We skip to derive the physical parameters of the outflow as it is heavily mixed with background emission, and we did not study other outflow (IRAS 23032+5937) in detail. Spectra of several molecular lines of IRAS 23033+5951 are presented in Figure 10. Solid line is ^{12}CO, dash-dot line is ^{13}CO, dash line is CS, and dotted line represents C^{18}O. CS and C^{18}O emission are multiplied by three times to show up their features to be compared.

(e) CS and C^{18}O

CS molecule is known to be a good tracer of dense molecular gas. The CS peak temperature map is presented in Figure 11. According to this CS map, there are several dense cores which are not directly affected by the H II region, and thus not enough heated by

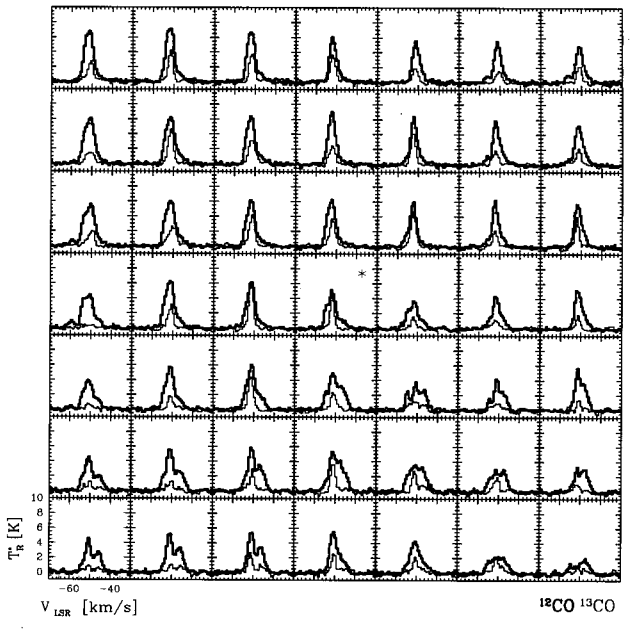

Fig. 9.— The ^{12}CO and ^{13}CO composite spectra observed around IRAS 23032+5937. The thick line is for ^{12}CO, and the thin line is for ^{13}CO. The spacing between each panel is 2 arcminutes. Asterisk mark is the position of the IRAS point source associated with the outflow.

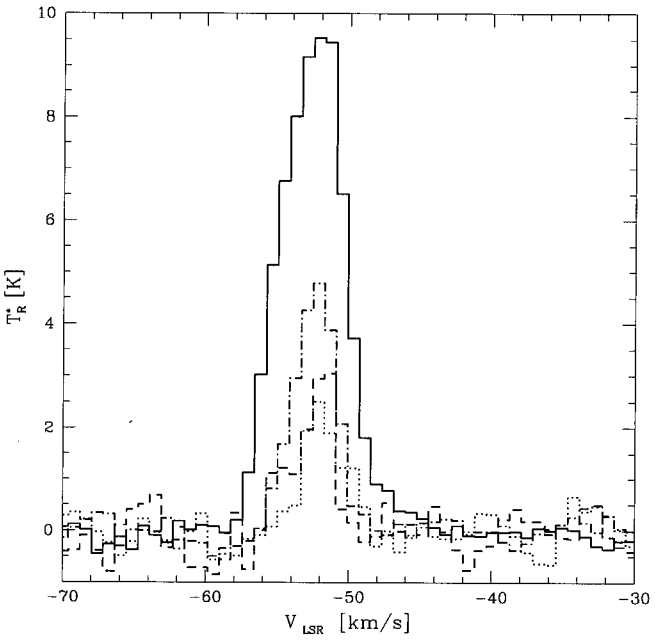

Fig. 10.— Spectra of several molecular lines of IRAS 23033+5951. Solid line is ^{12}CO, dash-dot line is ^{13}CO, dash line is CS, and dotted line represents C^{18}O. CS and C^{18}O emission are multiplied by three times to show up their features to be compared.

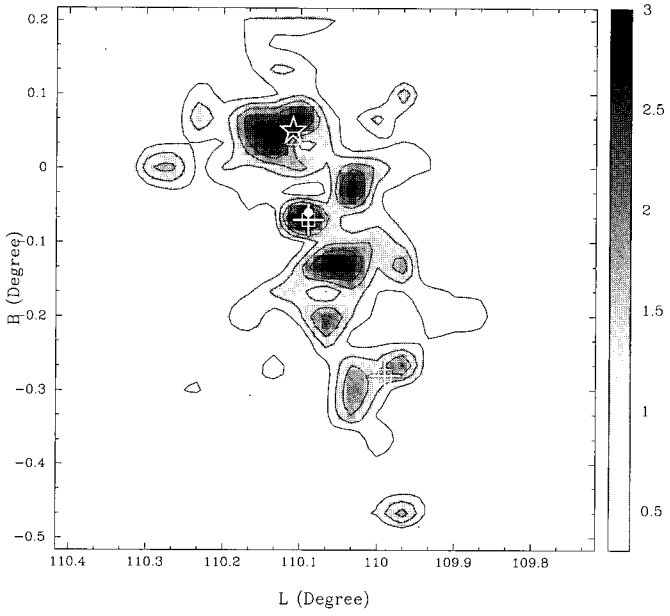

Fig. 11.— The CS peak temperature map. The symbols are as in Fig. 2. The starting contour is 0.4 K, and the contour increment is 0.2 K.

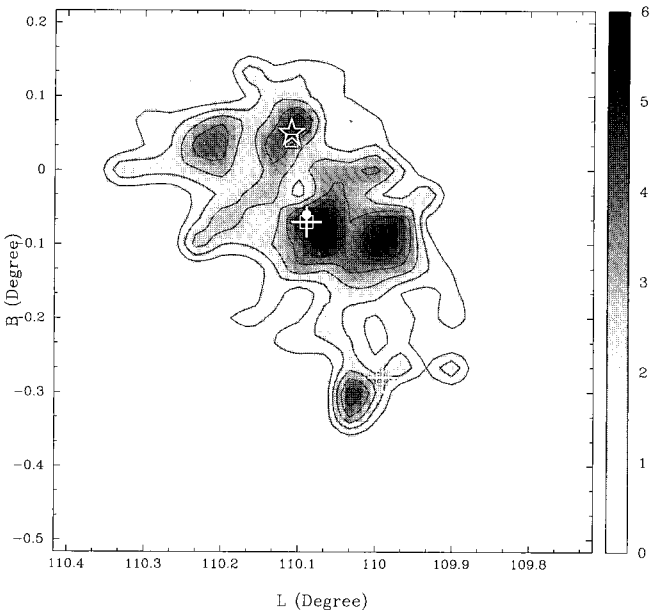

Fig. 12.— The $C^{18}O$ integrated intensity map. The symbols are as in Fig. 2. The starting contour is 0.5 K km s^{-1}, and the contour increment is 0.5 K km s^{-1}.

H II region. Some IRAS point sources and MXS point sources are found toward these cores (see Figure 4). The CS emission at $(l, b) = (110.°1\ , -0.°07)$ is stronger than main H II region. At this position there is a relatively strong IRAS point source IRAS 23033+5951. $S_{100} = 1,830$ Jy, and $S_{60} = 316$Jy. As the flux at 100 μm is larger than S_{60}, it is surely an embedded object. A few other IRAS point sources have the same trend. FIR luminosity was calculated for IRAS 23033+5951 using the following equation (Lonsdale & Helou 1985):

$$L_{FIR} = 4\pi d^2[1.26R(1.00 \times 10^{12} S_{100} + 2.58 \times 10^{12} S_{60})], \quad (2)$$

where S_ν is the flux density at IRAS band ν, d is the distance to the object, and R is the color correction factor. With the distance of 3.5 kpc and the correction factor of 1.5 (Lonsdale & Helou 1985), its FIR luminosity is estimated to be $1.9 \times 10^4 L_\odot$, which is close to that of Herbig Be star. Figure 12 is $C^{18}O$ integrated intensity map for the (−55.12, −44.88) km s^{-1}. $C^{18}O$ integrated intensity map shows a similar trend as CS emission map does. These cores seem to be good candidates of smaller star-forming regions.

IV. DISCUSSION

The molecular gas associated with the H II region Sh 156 has an elongated morphology, about 60 degrees tilted with respect to the Galactic plane. Several clumps/cores are found to reside within it, many of which are matching with MXS and IRAS point sources: There are at least three conspicuous ^{13}CO peaks at $(l, b) = (110.°0$ to $110.°1, -0.°1)$. These are also the densest part of the cloud (see Figures 11 and 12). In addition, we examined the continuum map at 11cm obtained from the MPIfR's Survey Sampler for the target region, which traces the distribution of the ionized gas. Beside the strong continuum emission from the H II region, we found an enhanced continuum feature, which was designated as $G110.25+0.01$ by Israel et al. (1978), though its emission strength is much weaker than that of the H II region Sh 156. Barlow et al. (1976) suggested that an early type (B5) star is located on this small continuum peak. Around this region we detected quite strong ^{13}CO emission of 4.8 K at $(l, b) = (110.°3, 0.°0)$. Thus, it is very likely that more star forming activities seem to be going on along with the H II region itself and the outflow. Because of the background contamination, we were not able to justify whether these are T Tauri stars or Herbig Ae/Be stars. However, there is at least one Herbig Be star candidate (IRAS 23033+5951), which is the strongest IRAS point source except the region directly associated with the H II region. Others could be T Tauri stars.

Even though there is a significant sign that the velocity field of the cloud is affected by the H II region, as shown in Figures 7 and 8, the associated molecular gas is not severely disturbed by the H II region Sh 156, and it does seem to be gravitationally bound, thus and virialized. From the definition of two components of velocity dispersions, the internal velocity dispersion, σ_i, and the centroid velocity dispersion, σ_c, which are estimated as 2.19 km s^{-1} and 1.14 km s^{-1}, respectively, the virial equilibrium status of the cloud can be discussed. The internal velocity dispersion of target cloud

is found to be more than twice larger than its centroid velocity dispersion. This fact implies that the turbulent, or bulk motions within individual clouds are not as significant as their internal thermal motions. This fact also support the virial equilibrium and thus, virial mass estimate is valid for this cloud (see below).

In most cases, there are some mass discrepancy in three different mass estimate techniques, whether a molecular cloud is in virial equilibrium or not. Several uncertainties are usually involved in each technique: virial mass, LTE mass, and a mass using a conversion factor (M_{CO}). Virial mass estimate is based on the virial equilibrium assuming a gravitational bound system, not including the external pressure for simplicity. Most of giant molecular clouds are known to be in virial equilibrium, even though they are associated with H II regions (Scoville et al. 1987). The target object in this study also shows that its internal velocity dispersion is substantially larger than the centroid velocity dispersion, and that virial mass is estimated to be the same as the M_{CO}. Thus, the the molecular cloud is likely in virial equilibrium, even without considering the external pressure, and the uncertainty involved in these two mass estimates would be minimal.

In the meanwhile, as ^{13}CO emission is usually weaker than ^{12}CO emission for all the clouds, the LTE mass is substantially smaller than the other estimates (Lee & Jung 2003). For our target cloud, the LTE mass is 20-30 % smaller than other estimates, as expected. The discussion about the mass discrepancy can be found also in Lee (1994). He claimed that the mass estimate using a conversion factor, M_{CO}, can be the best choice, especially when the cloud is not virialized. However, for our target cloud, M_{CO} is similar M_{VIR}, which means H II region ionized by O7 star is sufficient to heat up molecular gas, but not enough to disturb the associated molecular cloud in large scale, and the molecular cloud seems to be gravitationally bound.

V. SUMMARY

We presented the results of an observational study of the molecular cloud associated with Sh 156. The main results of this study are summarized as follows:

(1) We have mapped a $40' \times 42'$ region including Sh 156 using the TRAO 14m telescope in ^{13}CO, C^{18}O, and CS, and combined with Outer Galaxy Survey ^{12}CO data. The sampling grid was $2'$ and the beam size is $53''$ at ^{13}CO.

(2) The molecular cloud is confirmed to be associated with the H II region Sh 156; Line profiles are broadened around the H II region, implying that it is directly affected by the stellar wind from the H II region Sh 156.

(3) M_{CO} is similar to M_{VIR}, implying that the H II region ionized by O7 star is sufficient to heat up molecular gas, but not enough to disturb the whole extent of the associated molecular cloud. The centroid velocity dispersion of the cloud is substantially smaller than its internal velocity dispersion, which also support the virial equilibrium status.

(4) Several clumps/cores are found to reside within the cloud, many of which are matching with MXS and IRAS point sources: There are at least three conspicuous ^{13}CO peaks, and these are also the densest part of the cloud. It is very likely that other star forming activities seem to be going on along with the H II region itself and the outflow.

ACKNOWLEDGEMENTS

This work was supported by grant R01-2003-000-10513-0 from the Basic Research Program of the Korea Science and Engineering Foundation (KOSEF).

REFERENCES

Barbon, R., & Hassan, S. M., 1996, A new study of the young open cluster NGC 7510, A&AS,115, 325

Barlow, M. J., Cohen, M., & Gull, T. R., 1976, Extinction variations in the H II regions Sharpless 156 and 162, MNRAS, 176, 359

Blair, G. N., Peters, W. L., & vanden Bout, P. A., 1975, Strong molecular line emission associated with small Halpha emission regions, ApJ, 200, 161

Blitz, L., Fich, M., & Stark, A. A., 1982, Catalog of CO radial velocities toward galactic H II regions, ApJS, 49, 183

Cohen, M., & Barlow, M. J., 1973, Infrared Observations of Two Symmetric Nebulae, ApJ, 185, 37

Crampton, D., Georgelin, Y. M., & Georgelin, Y. P., 1978, First optical detection of W51 and observations of new H II regions and exciting stars, A&A, 66, 1

Dickman, R. L., 1978, The ratio of carbon monoxide to molecular hydrogen in interstellar dark clouds, ApJS, 37, 407

Elmegreen, B. G., & Moran, J. M., 1979, Observations of the shock in a region of shock-induced star formation - NGC 281, ApJ, 227, 93

Elmergreen, B. G., & Wang, M., 1987, in Molecular Clouds in the Milky way and External Galaxies, ed. R. L. Dickman, R. L. Snell., & J. S. Young (Berlin: Springer), 240

Fich, M., Treffers, R. R., & Dahl, G. P., 1990, Fabry-Perot H-alpha observations of Galactic H II regions, AJ, 99, 622

Fürst, E., Reich, W., Reich, P., & Reif, K., 1990, A Radio Continuum Survey of the Galactic Plane at 11-CENTIMETER Wavelength - Part Three - the Area 76 DEG < L < 240 DEG, A&AS, 85, 691

Heydari-Malayeri, M., Testor, G., & Lortet, M. C., 1980, Interaction of hot stars and the interstellar matter. X - Morphology, excitation, and structure of the bright galactic nebula Sh2-156 /IC 1470/, A&A, 84, 154

Heyer, M. H., Brunt,C., Snell, R. L., Howe, J. E., Schloerb, F. P., & Carpenter, J. M., 1998, The Five College Radio

Astronomy Observatory CO Survey of the Outer Galaxy, ApJS, 115, 241

Hodapp, K-W., 1994, A K′ imaging survey of molecular outflow sources, ApJS, 94, 615

Hunter, D.A., & Massey, P., 1990, Small Galactic H II regions. I - Spectral classifications of massive stars, AJ, 99, 846

Israel, F. P., 1978, H II regions and CO clouds - The blister model, A&A, 70, 769

Keto, E. R., & Ho, P. T. P., 1989, NH_3 observations of compressed postshock molecular gas in ionization-shock fronts around W33, ApJ, 347, 349

Kutner, M. L., & Ulich, B. L., 1981, Recommendations for calibration of millimeter-wavelength spectral line data, ApJ, 250, 341

Lada, C. J., Elmegreen, B. G., Cong, H.-I., & Thaddeus, P., 1978, Molecular clouds in the vicinity of W3, W4, and W5, ApJ, 226, 39

Lee, Y., 1994, Mass estimate of molecular clouds, PKAS, 9(1), 55

Lee, Y., & Jung, J. H., 2003, A molecular cloud complex above the galactic plane. I. Extended CO observations of the NGC 281 region, New Astronomy, 8, 191

Lonsdale, Carol J., & Helou, G., 1985, Cataloged galaxies and quasars observed in the IRAS survey, (Pasadena: Jet Propulsion Laboratory)

Lynds, B. T., & O'Neil, E. J., Jr., 1983, An optical study of IC 1470, ApJ, 265, 803

Roh, D.G., & Jung, J. H., 1999, Characteristics of TRAO 14M Radio Telescope (1999), PKAS, 14, 123

Scoville, N. Z., Yun, M. S., Clemens, D. P., Sanders, D. B., & Waller, W. H., 1987, Molecular clouds and cloud cores in the inner Galaxy, ApJS, 63, 821

Schmidt, M., 1965, in Stars and Stellar Systems, Vol. 5, ed. A. Blaauw and M. Schmidt (Chicago: University of Chicago Press), 513

Smutko, Michael F., & Larkin, James E., 1999, A Morphological Study of Infrared Line Emission in Compact Star-Forming Regions, AJ, 117, 2448

Strong, A. W., & Mattox, J. R., 1996, Gradient model analysis of EGRET diffuse Galactic -ray emission, A&A, 308, L21

Tenorio-Tagle, G., 1979, The gas dynamics of H II regions. I - The champagne model, A&A, 71, 59

Valdettaro, R., Palla, F., Brand, J., Cesaroni, R., Comoretto, G., Di Franco, S., Felli, M., Natale, E., Palagi, F., Panella, D., & Tofani, G., 2001, The Arcetri Catalog of H_2O maser sources: Update 2000, A&A, 368, 845

Williams S. J., Fuller G. A., & Sridharan T. K., 2004, The circumstellar environments of HMPOs. I: Submillimetre continuum emission, A&A, 417, 115

Wouterloot, J. G. A., Henkel, C., & Walmsley, C. M., 1989, CO observations of IRAS sources in Orion and Cepheus, A&A, 215, 131

Wu, Y., Wei, Y., Zhao, M., Shi, Y., Yu, W., Qin, S., & Huang, M., 2004, A study of high velocity molecular outflows with an up-to-date sample, A&A, 426, 503